

Gas-phase hydrogen isotope absorption/adsorption characteristics of a Ni-based sample

Y. Miyoshi^{1*}, H. Sakoh¹, A. Taniike¹, A. Kitamura¹,
A. Takahashi², T. Murota³ and T. Tahara³

¹Graduate School of Maritime Sciences, Kobe University

²Osaka University, ³Santoku Corporation

*yuuki.miyoshi@gmail.com

Abstract: Using a nano-composite sample of Ni-Cu-Zr oxide, it has been confirmed that nickel does not make observable absorption of hydrogen at room temperature. Preliminary results show that absorption of both D and H is possible at a temperature above 373 K, and the loading ratios reach about 1.0 at 525 K. As for the heat balance, the endothermic tendency is observed both in D and H runs below 500 K, above which only D-gas run gave the exothermic tendency. At 523K, while the deuterium run remains endothermic, the protium run showed the exothermic tendency with a specific output energy reaching the anomalously large value of about 300 eV/atom-Ni. If this turns out to be a true exothermic phenomenon, it is suggested strongly that a nuclear process should participate in the phenomenon.

Keywords: nano-composite sample, hydrogen isotopes, absorption, Ni-Cu, exothermic,

1. Introduction

Usually nickel doesn't absorb hydrogen at room temperature. In the case of our Ni-ZrO₂ (NZ) sample nano-fabricated by Santoku Corporation, we haven't observed any absorption of hydrogen accompanied by exothermic temperature change [1,2]. Hydrogen absorption characteristics of the PNZ2B sample with a small fraction of Pd, Pd₁Ni₇ nano-particles dispersed in a ZrO₂ supporter, supplied by B. Ahern has shown a dramatic change, and the amount of absorbed hydrogen was very large [3,4,5]. This result gives us a great hint that significant improvement of absorption characteristics would be expected by adding a small amount of foreign atoms to the NZ sample.

Recently, Rossi and Focardi (see their Internet blog J. Nuclear Physics) made a demonstration to appeal large and persistent heat generation on the order of kW from a Ni-based alloy powder sample absorbing protium (H)-gas at elevated temperatures over 573 K. Brian Ahern infers that their sample would be a mixture of Ni and Cu. In the present study, we used a ternary compound of Cu-Ni-Zr mixed oxide ("CNZ") nano-fabricated by Santoku Corporation as a sample for hydrogen isotope absorption experiments. Preliminary results implying anomalously long-lasting endothermic/exothermic characteristics are shown below.

2. Experimental apparatus and preparatory absorption runs

Physical properties of the sample are tabulated in Table 1. The experimental setup is shown schematically in Fig. 1. The system is composed of two identical chambers,

Table 1. Characteristics of the CNZ sample.

	Cu	Ni	Zr
Specific surface area [m^2/g]	45.3		
Composition [%]	7.9	56.1	36.0
Average grain size of oxide [nm]	6.8	24.5	---

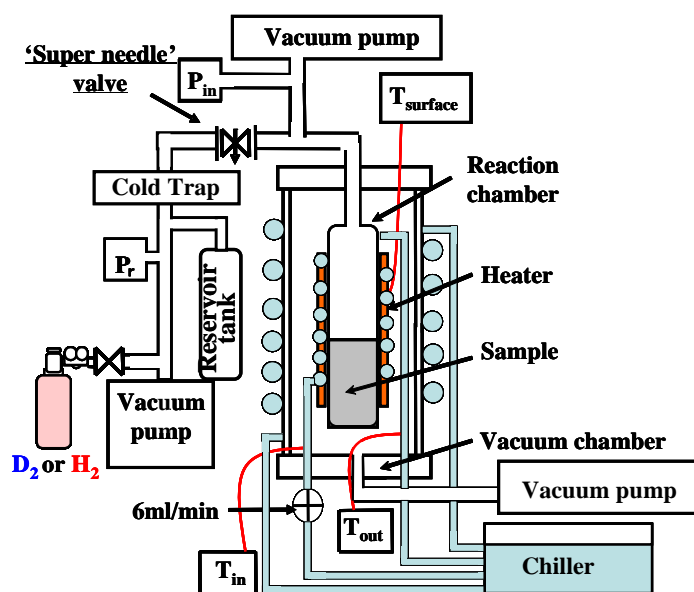


Fig. 1. Functional view of the system $A_1 \cdot A_2$. Water cooling of the reaction chamber with a flow rate of 6 ml/min was done only in the #1 run at room temperature, while the pipe was emptied of the cooling water in the #5 runs at elevated temperatures.

each of which contains a reaction chamber connected to an independent gas supply system. Three thermocouples per each chamber are set up to provide isothermal calorimetry data, at a middle point of the outer surface of the reaction chamber, a bottom point and a point near the flange of the outer vacuum chamber for thermal isolation. Two outer vacuum chambers of the twin system were cooled by water kept at a regulated temperature of 20 ± 0.1 °C. The laboratory was air-conditioned to keep room temperature at 20 ± 0.1 °C. As blank runs of isothermal calorimetry, He-4 gas charging runs instead of H(D)-gas runs were done to take correction data for time-evolutions of the temperature and the pressure in the reaction chamber. To elevate temperature, ohmic heating was used. Time variation of input powers were routinely registered and used for correction in calorimetry calculations. Any fluctuation of the temperature of the reaction chamber not coincident with intentional change in the heater input power is regarded as a systematic error, and was evaluated to be ± 0.2 W. An example of such fluctuations is seen in Fig. 3 shown later. And the amount of absorbed hydrogen atoms in each reaction chamber can be calculated momentarily by measuring pressures of both the reaction

chamber and the reservoir tank.

Ten-gram aliquots of the as-received CNZ sample set up in each reaction chamber have been baked at 440 K for 2 hours in vacuum, and subjected to D₂ and H₂ absorption runs (#1 runs) first at room temperature. Figure 2 shows typical variation of the thermal output power data, $W_D(t)$ and $W_H(t)$, pressure data in the reaction chambers, $P_D(t)$ and $P_H(t)$, in units on the left vertical axis, and the time-dependent loading ratios, $L_D(t)$ and $L_H(t)$ in units on the right vertical axis, in the runs D-CNZ1 and H-CNZ2, respectively. Table 2 shows time-integrated parameters in these runs; the specific output energy $E_{D(H)}$ is the time-integrated output power per 1.0-g of nickel, and the loading ratios D(H)/Pd shown are the finally (in the end of run) attained values of $L_{D(H)}(t)$.

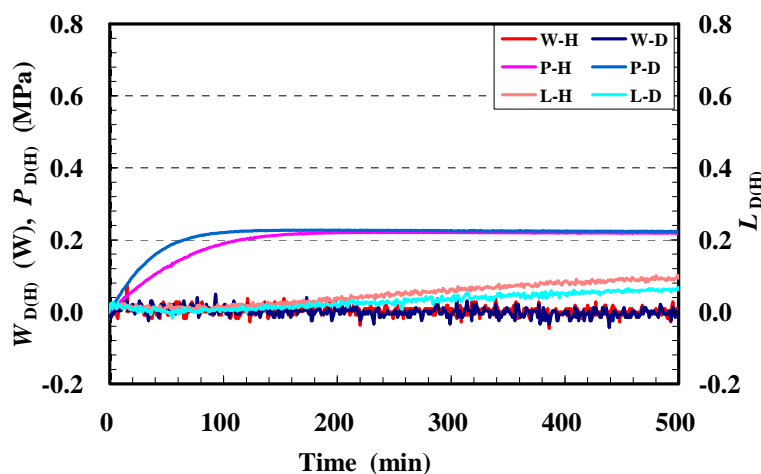


Fig. 2. Results of D₂/H₂ absorption runs for Cu·Ni·Zr oxide compounds at 300K; the run numbers are D-CNZ1#1 and H-CNZ2#1.

Table 2. Time-integrated parameters in the #1 runs at room temperature.

Run number	Duration [h]	Output energy E [kJ]	Specific output energy $E_{D(H)}$ [eV/atom-Ni]	Averaged output power $W_{D(H)}$ [W]	Loading ratio D/Ni, H/Ni
D-CNZ1#1	8.33	0.00	0.00	0.00	0.06
H-CNZ1#1	8.33	0.13	0.04	0.00	0.09

These runs at room temperature, D-CNZ1#1 and H-CNZ2#1, have given small, effectively negligible, D(H) absorption rate and thermal power evolution. This fact makes us confirm that nickel even in nano-powder has negligible effect on the hydrogen absorption nor heat evolution at room temperature.

However, activation of the H(D)-gas absorption reaction is expected at higher temperature. Therefore, the experiments were also conducted at elevated temperatures up to 573 K with use of the heater input power of up to 105 W.

In the high temperature runs, since the conventional water mass flow calorimetry cannot be used, the thermal output power was measured by the change in the temperature of the reaction chamber in comparison with a blank run using inert gas

instead of hydrogen isotopes. In order to make influence of environmental temperature change as small as possible, only the outer vacuum vessel was cooled with constant temperature water (regulated within 0.1 °C variation) and the experimental room was air-conditioned to keep temperature change within 0.1 °C variation. In order to obtain a calibration curve for the relation between the temperature and the colorific power, the temperature of the reaction chamber was measured for the heater input powers of 0 W, 15 W, 27 W, 43.5 W, 70 W, and 105 W. The results are shown in Table 3. Linear interpolation using the derivatives, $\Delta T/\Delta W$ values, is applied for an arbitrary value of

Table 3. Relation between the temperature of the reaction chamber and the heater input power for each subsystem, A₁ and A₂. The differential value $\Delta T/\Delta W$ is the slope of the line connecting the neighboring points.

Input power [W]	T [K]		$\Delta T/\Delta W$	
	A ₁	A ₂	A ₁	A ₂
0.0	294.2	294.2	---	---
15.0	393.3	388.2	6.61	6.27
27.0	435.9	429.3	3.55	3.43
43.5	480.7	472.1	2.72	2.59
70.0	524.5	523.2	1.65	1.93
105.0	559.2	558.0	0.99	0.99

the temperature other than the temperatures measured in the calibration.

When a gas is introduced through the cold trap (for impurity removal) into the reaction chamber maintained at a specified elevated temperature, the temperature falls off due to the effect of cooling. Therefore, blank runs in which ⁴He gas was introduced into the reaction chamber under the same experimental conditions as in the cases of the hydrogen runs were performed. An example of the blank run using ⁴He operated at 70 W is shown in Fig. 3. The fall of temperature, with the difference in the heat capacity of

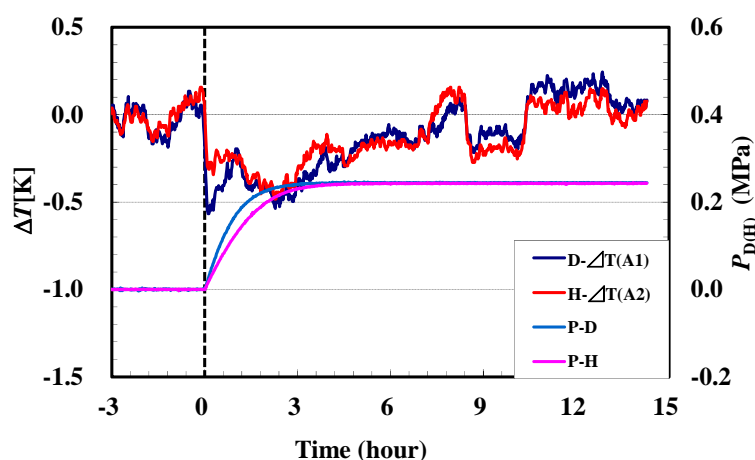


Fig. 3. Variation of temperature and pressure in the blank runs with ⁴He gas, at an input power of 70 W by the heater.

He and $D(H)_2$ taken into account, is used for correction in the data processing to obtain the thermal output power $W_{D(H)}(t)$.

The time-dependent hydrogen loading ratio $L_{D(H)}(t)$ is calculated from the difference in the total amount of the hydrogen gas indicated as the pressure data at the reservoir cylinder and the reaction chamber for the A_1 or A_2 subsystem, before and after introduction of the gas. Just after the introduction of the cooling gas, an apparent reduction in the loading ratio is caused by the expansion of the introduced cooling gas. The blank runs described above are used also for this purpose of corrections in the loading ratios, as well as the correction for the thermal power data. An example of the apparent loading ratio $L_{D(H)}(t)$ in the blank run using ^4He at 70 W is shown in Fig. 4. This apparent reduction in the loading ratio, with the difference in the heat capacity of He and $D(H)_2$ taken into account, is used in the data processing to calculate the time-dependent loading ratio $L_D(t)$. The effect of the difference in the heat capacity on the value of $L_{D(H)}(t)$ is 30 % at most.

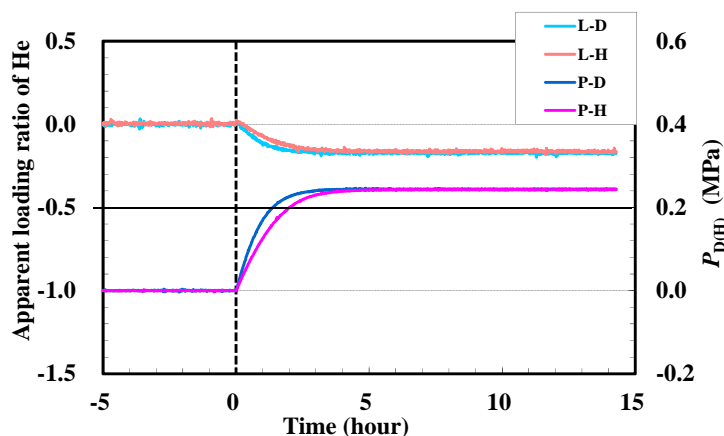


Fig. 4. Pressure and apparent loading ratio in the blank run with ^4He gas at an input power of 70 W from the heater.

3. Hydrogen absorption runs at elevated temperatures

The hydrogen gas absorption runs were conducted for the CNZ1(2) samples at temperatures of 373 K, 473 K and 523 K. After the #1 runs the CNZ1(2) samples in the A_1 and A_2 chambers were baked at 440 K for 3 hours in vacuum, and then subjected to the D_2 (H_2) absorption runs at 373K; $D(H)\text{-CNZ1}(2)_373\text{K}_1$. The baking-absorption run cycle was repeated four times with additional three runs at 473 K and 523 K; $D(H)\text{-CNZ1}(2)_5_373\text{K}_1$, $D(H)\text{-CNZ1}(2)_5_473\text{K}_1$, $D(H)\text{-CNZ1}(2)_5_525\text{K}_1$ and $D(H)\text{-CNZ1}(2)_5_525\text{K}_2$. The time evolution data of the thermal output power $W_{D(H)}(t)$, the pressure in the reaction chamber $P_{D(H)}(t)$ and the loading ratio $L_{D(H)}(t)$

calculated from the pressures are shown in Fig. 5-(a) through (d), and Table 4 shows the time-integrated parameters of these runs, D(H)-CNZ1(2)#5_373K_1 through D(H)-CNZ1(2)#5_523K_2.

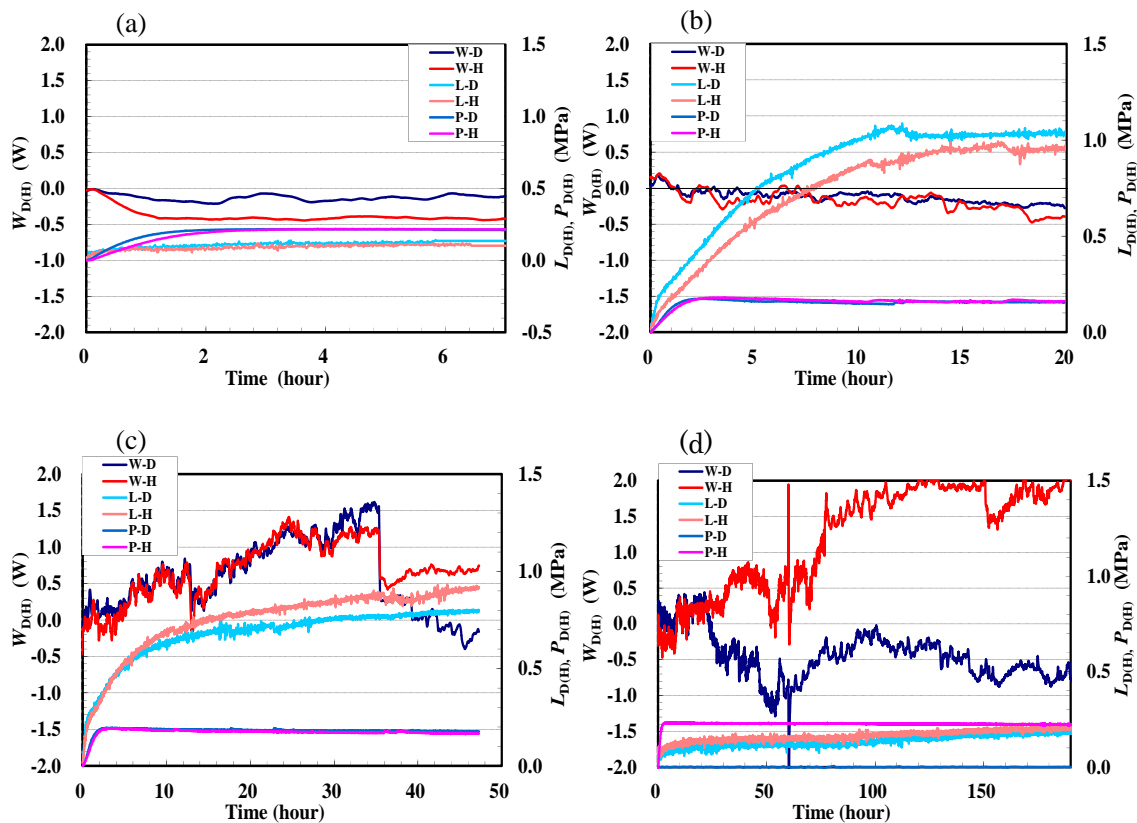


Fig. 5. Variation of the thermal output power $W_{D(H)}(t)$, the pressure $P_{D(H)}(t)$ and the time-dependent loading ratio $L_{D(H)}(t)$ in the runs (a) D(H)-CNZ1(2)#5_373K_1, (b) D(H)-CNZ1(2)#5_473K_1, (c) D(H)-CNZ1(2)#5_523K_1 and (d) D(H)-CNZ1(2)#5_523K_2.

Table 4. Time-integrated parameters in the runs D(H)-CNZ1(2)#5_373K_1, D(H)-CNZ1(2)#5_473K_1, D(H)-CNZ1(2)#5_523K_1 and D(H)-CNZ1(2)#5_523K_2..

Run number	Duration [h]	Amount of Ni	Specific output energy	Averaged output power	D.Ni or H/Ni
D-CNZ1#5_373K_1	7.0	2.0	-1.06	-0.06	0.14
H-CNZ2#5_373K_1			-3.18	-0.19	0.10
D-CNZ1#5_373K_2	21.2	2.0	-6.58	-0.13	0.06
H-CNZ2#5_373K_2			-7.26	-0.14	0.06
D-CNZ1#5_473K_1	20.2	2.0	-2.86	-0.06	1.04
H-CNZ2#5_473K_1			-4.17	-0.09	0.97
D-CNZ1#5_523K_1	47.4	2.0	33.0	0.29	0.79
H-CNZ2#5_523K_1			38.7	0.34	0.92
D-CNZ1#5_523K_2	191.3	2.0	-103	-0.23	0.18
H-CNZ2#5_523K_2			278	0.61	0.21

Absorption of hydrogen was observed by heating-up a CNZ sample to 373K. However, it showed an endothermic behavior as a whole. In the D(H)-CNZ1(2)#5_473K_1 runs the loading ratio increased sharply reaching to about 1.0. Although the thermal output power became positive slightly in the early stage of the run, it showed an endothermic tendency as a whole. At 523 K the loading ratio of about 1.0 was reproduced, and the prolonged exothermic tendency continued for 47 hours. Although it is only a small change compared with the input heater power of 69 W, the output energy is 19.3 (29.6) eV/atom-Ni, respectively for the D(H)-run, when the power is time-integrated up to 2000 min. This is a very big generation of heat.

In order to check the reproducibility of the large loading ratio and the prolonged exothermic tendency shown in D(H)-CNZ1(2)#5_523K_1, the last run (523 K_2) was done at the same temperature. The Loading ratios in the repeated runs reached only to 0.24 and 0.25 for D and H, respectively, and the thermal output power data showed quite different behavior. While the power $W_H(t)$ for protium increased up to 2 W, $W_D(t)$ for deuterium turned back even to negative. While the time-integrated power E_H (the output energy for protium) was calculated to be 2.8×10^2 eV/atom-Ni, that for deuterium E_D was negative (-1.0×10^2 eV).

It seems that the repeated runs D(H)-CNZ1(2)#5_523K_2 should be regarded as extensions of the D(H)-CNZ1(2)#5_523K_1 runs, since the baking process seems to have had little effect on the initial conditions of the D(H)-CNZ1(2)#5_523K_2 runs. This is because the baking process done at the temperature of 340 K is much lower than the operating temperature of 523 K in the D(H)-CNZ1(2)#5_523K_1 and D(H)-CNZ1(2)#5_523K_2 runs. If this is the case, and if no consideration related to the baking process is necessary, the overall loading ratios are summed up to D(H)/Ni = 1.1 (1.2), while the output energies are summed up to $E_{D(H)} = -1.4 \times 10^2$ (3.1×10^2) eV/atom-Ni for the operating period of 2.4×10^2 h.

As concluding figures for the hydrogen absorption runs using the Cu-Ni-Zr mixed oxide sample, Fig. 9 and Fig. 10 summarize the integrated behavior of the specific output energy and the loading ratio as a histogram. If this reflects a true aspect of the phenomenon, the exothermic reaction is only for protium and has a threshold temperature between 200 K and 250 K, as is said by other researchers (B. Ahern, F. Piantelli, private communications). Moreover, the value of the specific output energy E_H reaching about 300 eV/atom-Ni is too high to be explained only by known chemical processes.

(In the later experiments after JCF12, we have found that the D-gas data made catch-up to the H-gas exothermic thermal power level in the later time interval of

several weeks of long run-time. We will report it separately to the present report.)

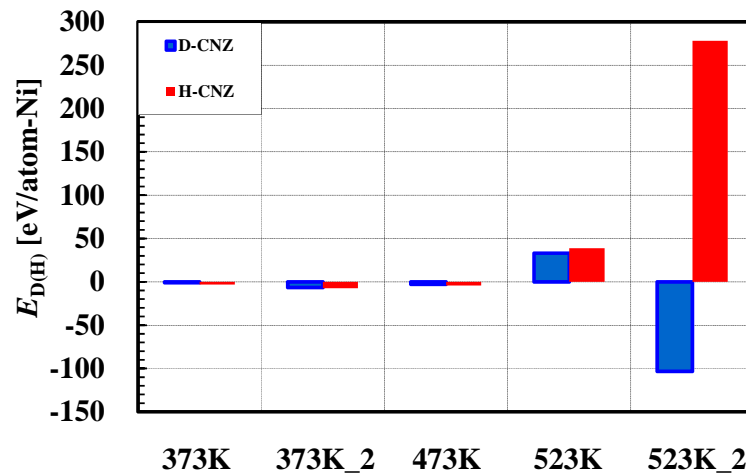


Fig. 6. Variation of the specific output energy E in the runs D(H)-CNZ1(2)#1 through D(H)-CNZ1(2)#5_523K_2.

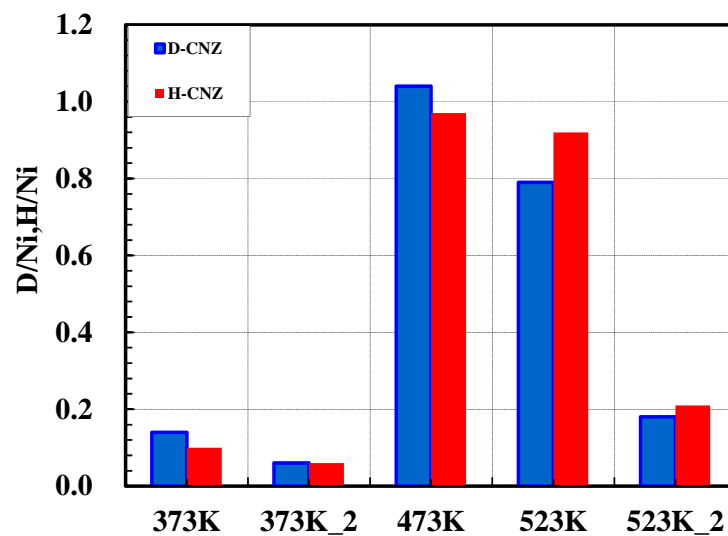


Fig. 7. Variation of the loading ratio D(H)/Ni in the runs D(H)-CNZ1(2)#1 through D(H)-CNZ1(2)#5_523K_2.

4. Summary

It has been confirmed that nickel nano-powder does not make observable absorption of hydrogen and generation of heat at room temperature. Absorption of both D and H became possible at elevated temperatures above 300 K, and the loading ratios D(H)/Ni reached about 1.0 at 523 K.

As for the heat balance, the endothermic tendency was observed both in D and H runs below 500 K, above which only H had the exothermic tendency. At 523K, while the deuterium run remained endothermic, the protium run showed the exothermic tendency with a specific output energy reaching about 300 eV/atom-Ni which is anomalously high in view of the known chemical reactions.

If this is a true exothermic phenomenon, it cannot be a simple chemical reaction caused by re-arrangement of orbital electrons for chemical compounds, and it is suggested strongly that some nuclear process participates in the phenomenon. It is necessary to advance extended experiments further to check the reproducibility of this phenomenon with D(H) isotope effects and to understand the underlying mechanisms.

References

- [1] Y. Sasaki, Y. Miyoshi, A. Taniike, A. Kitamura, A. Takahashi, R. Seto and Y. Fujita; Proc. JCF10 (2010) 14-19.
- [2] A. Kitamura, Y. Miyoshi, A. Taniike, A. Takahashi, R. Seto and Y. Fujita; J. Condensed Matter Nucl. Sci. 4 (2011) 56-68.
- [3] B. Ahern; private communication
- [4] H. Sakoh, Y. Miyoshi, A. Taniike, A. Kitamura, A. Takahashi, R. Seto and Y. Fujita; Proc. JCF11 (2011) 16-22.
- [5] Y. Miyoshi, H. Sakoh, A. Taniike, A. Kitamura, A. Takahashi, R. Seto and Y. Fujita; Int. Conf. on Condensed Matter Nuclear Science, ICCF16, Chennai, 2011, paper MT-02.